Journal of The Electrochemical Society, **147** (2) 413-419 (2000)
S0013-4651(99)06-148-0 CCC: $7.00 © The Electrochemical Society, Inc.

Factors Controlling the Stability of O3- and P2-Type Layered MnO_2 Structures and Spinel Transition Tendency in Li Secondary Batteries

Sa Heum Kim,[a] Wan M. Im,[a] Jin K. Hong, and Seung M. Oh*,[z]

Division of Chemical Engineering and Institute of Chemical Process, College of Engineering, Seoul National University, Seoul 151-742, Korea

Cathode properties of two layered manganese dioxides ($A_xMnO_{2+\delta}\cdot yH_2O$, where A is the pillaring alkali cations) having different crystal structures were compared in 3 V Li secondary batteries. The materials were prepared from the mixture of KNO_3, LiOH, and MnO at 800 and 1050°C, respectively. The 800°C-prepared MnO_2 has a trigonal $R\bar{3}m$ space group with an O3-type oxide-packing pattern, whereas the 1050°C material has an orthorhombic *Cmcm* symmetry with a P2-type oxide-packing pattern. The gallery space where the pillaring cations and water molecules reside is wider in the case of the 800°C material. Due to the higher mobility of pillaring cations in the 800°C material and similarity in the oxide-packing pattern (O3-type) to the spinel phases, the pillaring cations are easily leached out during cell cycling, which ultimately leads to a lattice collapse and structural transition to the spinel-related phases. By contrast, as the 1050°C material has rather immobile pillaring cations and its oxide-packing pattern (P2-type) is far different from that of the spinel phases, this cathode shows better cycling performance, with its structural integrity being well maintained.
© 2000 The Electrochemical Society. S0013-4651(99)06-148-0. All rights reserved.

Manuscript submitted June 28, 1999; revised manuscript received September 27, 1999.

Transition metal oxides have been widely studied for the cathode materials in Li secondary batteries.[1-4] Among those, the spinel $Li_xMn_2O_4$ presents advantages over the layered Li_xCoO_2 or Li_xNiO_2 with a lower cost of Mn and easier preparation, but these advantages are largely offset by the lower rate capability, lower theoretical capacity, and higher cell voltage. The first feature comes from its three-dimensional tunnel structure where ionic diffusion during the charge/discharge reaction is more restricted than in the two-dimensional layered structures. The lower theoretical capacity in $Li_xMn_2O_4$ is caused by the narrower reversible range (x) for Li^+ intercalation/deintercalation. The higher cell voltage may be a problem because electrolytes can be decomposed during cell cycling.[5-7] In this sense, the layered MnO_2 (δ-MnO_2 or naturally occurring birnessite-related MnO_2) can be projected as an attractive candidate material because it combines in theory several advantageous features inherited from each oxide. It has a layered structure like Li_xCoO_2 and Li_xNiO_2, thereby, a high rate capability is expected. The lower cost of Mn is still a merit. In addition, its theoretical capacity is twice as large as the spinel assuming one-electron charge/discharge reaction in both materials. Finally, since the cell voltage of MnO_2 is known to be lower than the spinel $Li_xMn_2O_4$,[8] electrolyte decomposition is expectedly lower on these materials.

So far, there have been several attempts to apply layered MnO_2 to the cathode materials in Li secondary batteries, but the above-mentioned advantages are not fully assessed due to problems encountered in this material. The most serious problem with layered MnO_2 is, among others, their structural instability against the repeated lattice expansion/contraction with cell cycling.[9-12] Also, several reports complained that layered MnO_2 materials are susceptible to spinel transition.[12-15] It is thus likely that in order for layered MnO_2 materials to be successful for cathode application they should meet at least two requirements; the presence of immobile pillaring cations at the gallery space to maintain the layered framework and resistance against spinel transition.

In this study, we tried to prepare layered MnO_2 materials that have the above-mentioned characteristics via a high temperature solid-state reaction.[9-12] In the course of this study, we could fortuitously prepare layered MnO_2 phases of different crystal structures by adjusting the preparation temperature. The two MnO_2 phases differ in the size of gallery space such that the mobility of pillaring cations, and furthermore the stability of layered framework, expectedly differ from each other. In addition, since the two MnO_2 materials have different oxide-packing patterns, the spinel transition tendency is expectedly different between the two phases.[16] Structure-dependent cathode cyclability of layered MnO_2 is discussed.

* Electrochemical Society Active Member.
[a] Present address: Finecell Company, Limited, Kyungki-Do 463-070, Korea.
[z] E-mail: seungoh@plaza.snu.ac.kr

Experimental

Preparation and characterizations of layered MnO_2.—The layered MnO_2 materials were prepared by a thermal treatment of mixtures of KNO_3 (Aldrich, 99+ %), LiOH (Aldrich, 98+ %), and MnO (Aldrich, 99%) with an atomic ratio of K/Li/Mn = 5/1/10. For the synthesis, the precursor mixtures were first ballmilled, screened through a 400 mesh sieve (<63.5 μm), and pelleted (2.54 cm in diam, 1 mm thick). The pellets were then heat-treated at 800 or 1050°C in air for 2 h. The heating and cooling rates were controlled at 2 and 10°C min^{-1}, respectively. After the thermal treatment, the pellets were ground, washed with distilled water, screened through a sieve (<63.5 μm), and dried at 120°C under vacuum.

The crystal structure of the resulting powders was identified by X-ray diffraction (XRD) analysis (Cu Kα = 1.5418 Å) and further refined by the Rietveld method.[17] Details on the Rietveld refinement were reported in a previous paper.[11] The powder morphology was examined by scanning electron microscopy (SEM). The K, Li, and Mn contents were analyzed by the inductively coupled plasma (ICP) technique. The total Mn contents and average Mn valence were analyzed by potentiometric titration as reported in the literature.[18]

Electrochemical characterization.—To prepare the cathode, a pasted mixture of MnO_2 powder, Ketjen ECP600JD furnace black (Armak), and polytetrafluoroethylene (PTFE) binder (15:2:1 wt ratio) was pressed onto a stainless steel exmet (long width = 2 mm, short width = 1 mm, and apparent area = 1 cm^2), and dried at 120°C under vacuum. Li foil was used as the anode and reference electrode. The used electrolyte was PC + DME (1:1 volume ratio)/1 M $LiClO_4$ (Tomiyama), where PC is propylene carbonate and DME is dimethoxyethane. In order for the cell capacity to be limited by the cathode such that the observed capacity represents that of the cathode, an excess amount of Li metal was used as the anode. The galvanostatic charge/discharge behavior was analyzed (1 mA cm^{-2}, 0.4 C rate) within a voltage cutoff range of 2.0 to 4.3 V (*vs.* Li/Li^+). All the experiments were carried out at 25 ± 1°C in an Ar-filled dry box.

Results and Discussion

Preparation and structural analysis of layered MnO_2.—Figure 1 shows the thermogravimetry-differential thermal analysis (TG-DTA) profiles that were traced with a mixture of KNO_3, LiOH, and MnO

Downloaded 17 Jul 2009 to 147.46.182.184. Redistribution subject to ECS license or copyright; see http://www.ecsdl.org/terms_use.jsp

S0013-4651(99)06-148-0 CCC: $7.00 © The Electrochemical Society, Inc.

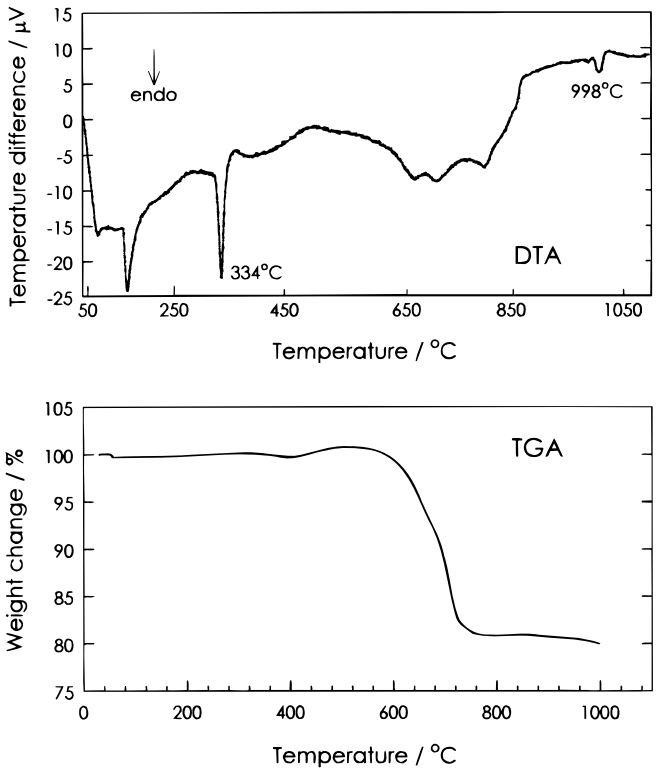

Figure 1. Thermogravimetric-differential thermal analyses curves obtained with a mixture of KNO_3, LiOH, and MnO (5/1/10 in atomic ratio). Note the endothermic peak at 998°C. The heating rate was 10°C min^{-1}.

(K/Li/Mn = 5/1/10 in atomic ratio). As shown, the dehydration takes place at 100 to 200°C and melting of KNO_3 at 330 to 340°C. As the reactant mixture decomposes at 600 to 750°C with a major weight loss, the preparation temperature was set at above 800°C. Also, as an endothermic peak was observed at 995 to 1000°C, which is seemingly related with a structural transition, the preparation was performed at two temperatures, before (800°C) and after (1050°C) the transition.

XRD powder patterns of the layered MnO_2 products are reproduced in Fig. 2, where it is seen that the lower angle (00*l*) peaks are stronger than the others, which may arise from a preferred orientation that is commonly observed in layered materials.[19,20] Figure 3 shows the SEM photographs of the prepared powders. As the XRD result suggests, the lamella-shaped crystals are well grown, indicating that the layers stack parallel to the (*a*,*b*) plane over large domains. As the preparation temperature increases, the growth of crystal size is apparent.

The Rietveld refinement was performed to assess the crystal structure for both materials. To avoid the problems encountered with the preferred orientation, the refinement was made at $2\theta = 30$ to 70°.[11] After a careful examination of the powder pattern of the 800°C material, a trigonal system (space group = $R\bar{3}m$),[21,22] rather than monoclinic[19,23-27] or orthorhombic[27,28] ones, was chosen as a start-

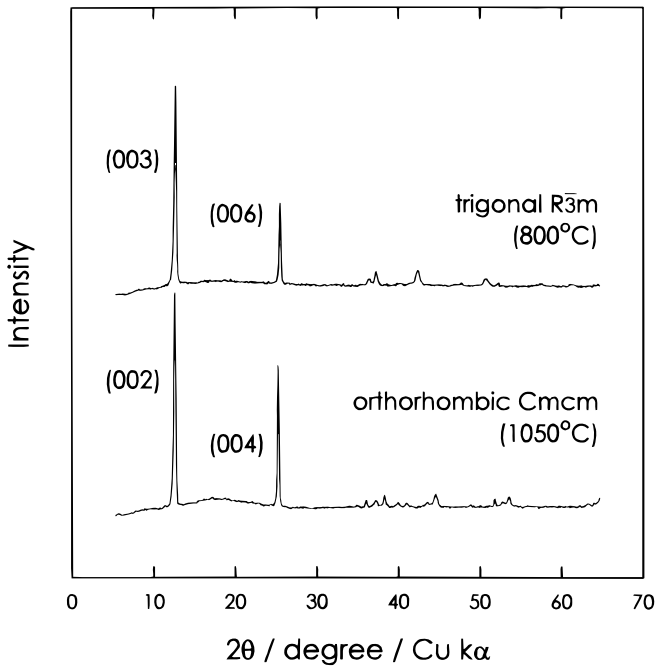

Figure 2. XRD powder patterns of the layered MnO_2 prepared at 800 and 1050°C. Note that the (00*l*) diffraction lines are dominant in each sample.

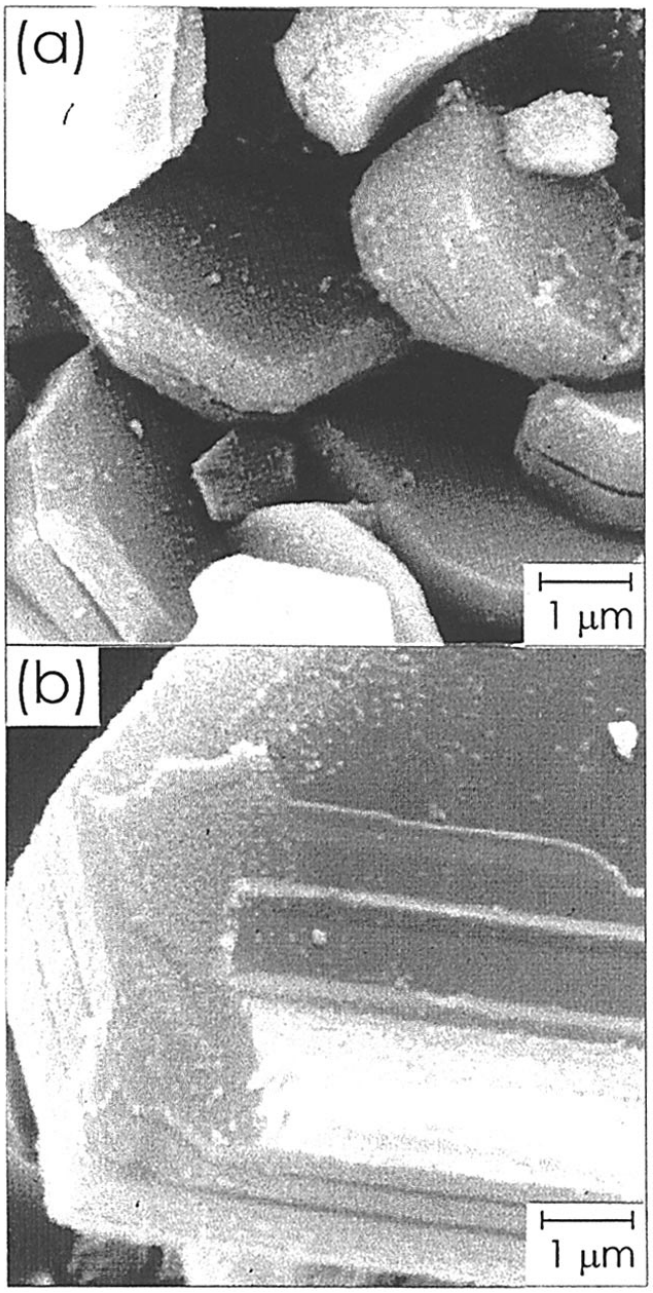

Figure 3. SEM photographs showing the crystal shape of MnO_2: (a) 800 and (b) 1050°C. Note the lamella-shaped crystallites.

Downloaded 17 Jul 2009 to 147.46.182.184. Redistribution subject to ECS license or copyright; see http://www.ecsdl.org/terms_use.jsp

S0013-4651(99)06-148-0 CCC: $7.00 © The Electrochemical Society, Inc.

ing model, with which all the diffraction lines except one at *ca*. 45° could be indexed with hexagonal axes. The data were further refined with reasonably small *R*-factors. The resulting crystallographic parameters are listed in Table I, and the calculated and observed diffraction profiles are presented in Fig. 4, where the calculated Bragg reflection positions are marked as the vertical bars. In the case of the 1050°C material, however, an orthorhombic unit cell (space group = *Cmcm*)[28] was chosen as the best starting model, with which all the diffraction lines except three at *ca*. 44, 53, and 56° could be indexed. The unindexed peaks are not fully characterized, but probably come from unknown impurity phases. The resulting crystallographic parameters are listed in Table I, and the calculated and observed diffraction profiles are displayed in Fig. 4.

Figure 5 shows the schematic drawing of the layered MnO_2 structure (800°C), which illustrates that the manganese ions in the layer plane (3 Mn in 3*b* (0 0 1/2) site) are octahedrally coordinated, and that the oxide ions in the layer plane [6 O in 6*c* (0 0 0.2034) site] provide the octahedral sites (3*a* (0 0 0) site) for the K^+ and Li^+ ions and H_2O in the gallery space. Thus, the stacking pattern parallel to the *z* axis can be described as *AcBa′CbAc′BaCb′* (O3-type), where *A*, *B*, and *C* represents the positions of the oxide ions, *a*, *b*, and *c* the positions of the manganese ions, and *a′*, *b′*, and *c′* the positions of K^+ and Li^+ ions and H_2O (Fig. 5b).

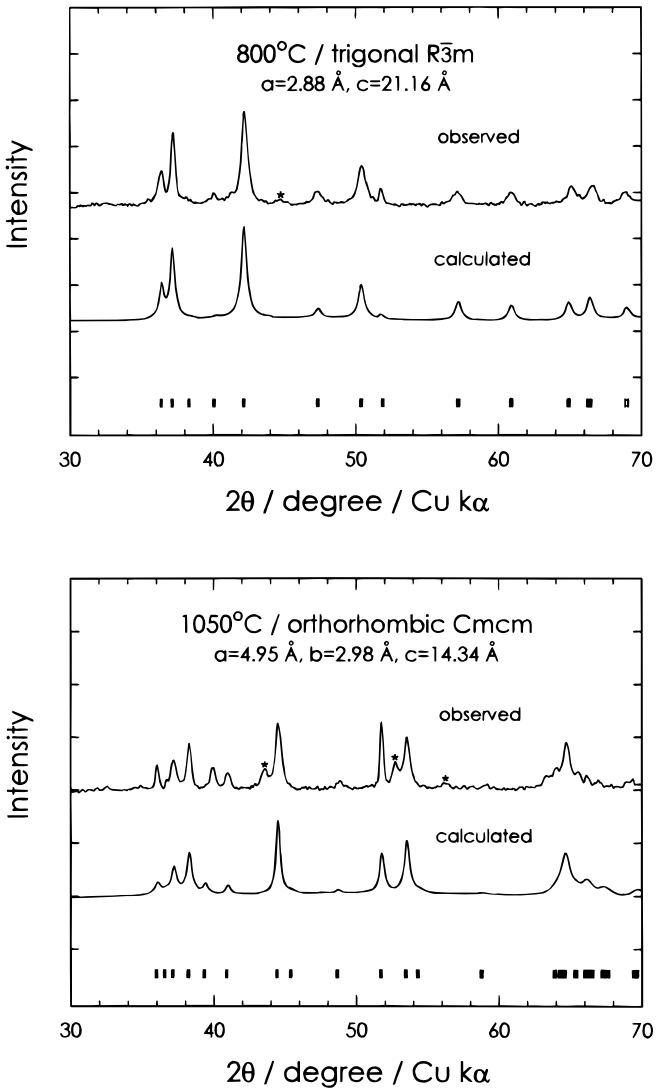

Figure 4. Results of Rietveld refinement on the layered MnO_2. The unindexed peaks were marked as (*). The crystallographic parameters were listed in Table I.

Table I. Crystallographic parameters of two layered MnO_2 materials.

	Preparation temperature (°C)	
	800	1050
Formula	$Li_{0.13}K_{0.34}MnO_{2.19}\cdot 0.27H_2O$	$Li_{0.12}K_{0.35}MnO_{2.14}\cdot 0.45H_2O$
Crystal system	trigonal [a]	orthorhombic
Space group	$R\bar{3}m$ (No. 166)	*Cmcm* (No. 63)
Cell parameters		
a	2.875(3) Å	4.953(5) Å
b		2.979(1) Å
c	21.16(1) Å	14.34(1) Å
c/*a*	7.361	2.895
a/*b*		1.663
Cell volume	151.4 Å^3	211.8 Å^3
Calculated density	3.58 g cm^{-3}	3.51 g cm^{-3}
Atoms		
Mn	3*b* (0 0 1/2) 97(1)% [b]	4a (0 0 0) 96(2)%
O	6*c* [0 0 0.2034(3)] 100%	8*f* [0 0.5904(4) 0.1019(3)] 100%
K, Li	3*a* (0 0 0) 45(2)%	4*c* [0 0.2084(3) 1/4] 46(2)%
Thermal factor [c]	0.23(2) Å^2	0.12(3) Å^2
R-factors [d] (%)		
R_p	1.29(1)	1.86(1)
R_{wp}	1.79(1)	2.64(1)
$R_{expected}$	3.85(2)	3.98(2)
R_{Bragg}	12.7(2)	15.6(2)

[a] Hexagonal axes were used for indexing.
[b] Occupancy.
[c] Overall isotropic temperature factors were used.
[d] *R*-factors

$R_p = 100\ \Sigma|y_i - y_{ci}|/\Sigma|y_i|$ pattern *R*-factor
$R_{wp} = 100\ (\Sigma\ w_i(y_i - y_{ci})^2/\Sigma\ w_i y_i^2)^{1/2}$ weighted pattern *R*-factor
$R_{expected} = 100\ [(N - P + C)/\Sigma\ w_i y_i^2)^{1/2}$ expected *R*-factor
$R_{Bragg} = 100\ \Sigma|I_o - I_c|/\Sigma|I_o$ Bragg *R*-factor

where, y_i, y_{ci}, and w_i are the observed and calculated intensity and weighted factor at each sampling step, respectively, and N, P, and C are the numbers of observation, refined parameters, and constraints, respectively, and I_o and I_c are the observed and calculated intensity at each Bragg reflection position.

The 1050°C material has the P2-type layered structure as shown in Fig. 6. In this scheme, the manganese ions in the layer plane (4 Mn in 4*a* (0 0 0) site) are octahedrally coordinated, and the oxide ions in the layer plane [8 O in 8*f* (0 0.5904 0.1019) site] provide the trigonal prismatic sites [4*c* (0 0.2084 1/4) site] for the K^+ and Li^+ ions and H_2O in the gallery space. Thus, the stacking pattern parallel to the *z* axis can be described as *AaBa′BbAb′* (P2-type), where *A* and *B* represent the positions of the oxide ions, *a* and *b* the positions of the manganese ions, and *a′* and *b′* the positions of K^+ and Li^+ ions and H_2O (Fig. 6b).

A comparison of Fig. 5b and 6b reveals that the 800°C-prepared MnO_2 has a longer O-K-O interplane distance (5.50 Å) than the 1050°C one (4.25 Å). For the O-Mn-O interplane distance, however, the 800°C material shows a shorter distance (1.55 Å) than the 1050°C one (2.92 Å). This illustrates that the gallery space is more spacious in the 800°C material, but the MnO_6 octahedra are considerably compressed along the *z* axis. It is thus likely that the binding force between the pillaring cations and the negatively charged oxide layer is stronger in the case of the 1050°C material.[29]

Downloaded 17 Jul 2009 to 147.46.182.184. Redistribution subject to ECS license or copyright; see http://www.ecsdl.org/terms_use.jsp

S0013-4651(99)06-148-0 CCC: $7.00 © The Electrochemical Society, Inc.

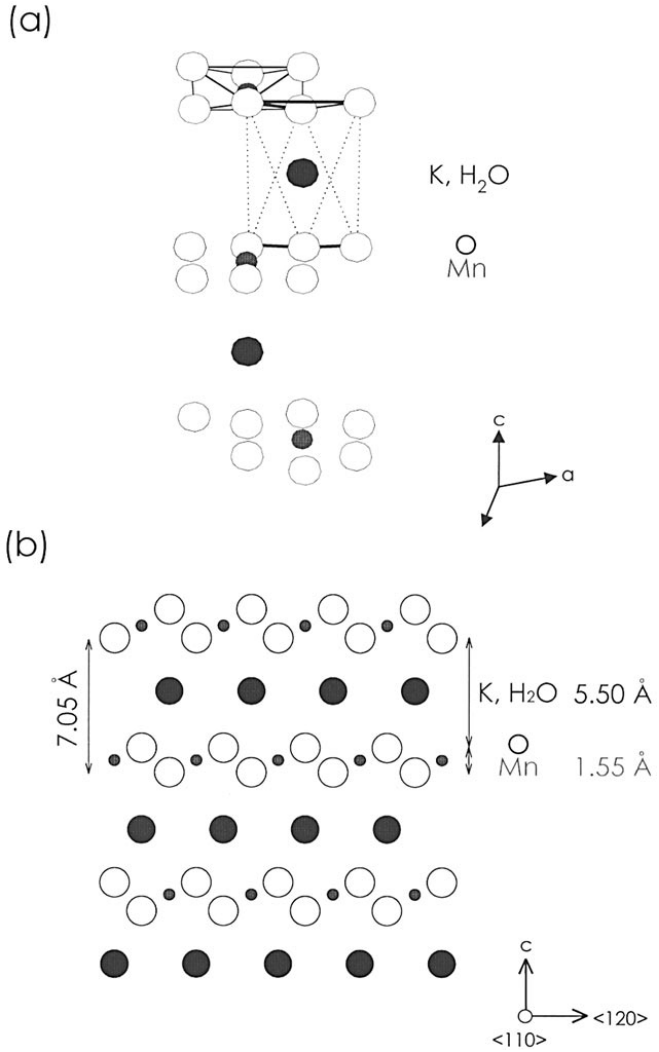

Figure 5. Schematic illustration of the layered MnO_2 structure prepared at 800°C: (a) three-dimensional view illustrating the position of alkali metal ions, and (b) <110> projection indicating the O3-type stacking pattern.

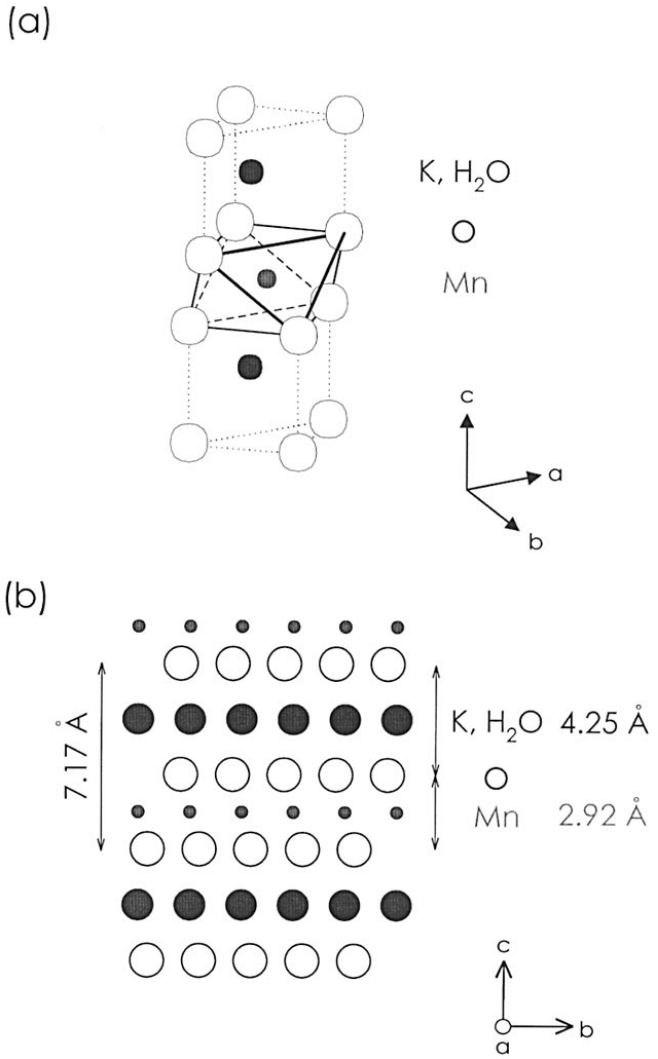

Figure 6. Schematic illustration of the layered MnO_2 structure prepared at 1050°C: (a) three-dimensional view showing that Mn ions are located in octahedral sites and alkali metal ions/H_2O in trigonal prismatic sites, and (b) <100> projection indicating the P2-type stacking pattern.

In order to estimate the mobility of pillaring cations, the materials were simply soaked in electrolytes, and the structural change was examined. As shown in Fig. 7, when the 800°C material is soaked in the electrolytes, there appears a substantial change in the diffraction patterns with some new diffraction lines being developed. This observation is contrasted by the negligible change in the 1050°C material. The chemical analysis made after the soaking experiment indicates that the leaching of K^+ ions is notably higher from the 800°C material, illustrating that the pillaring species in this material are so loosely bound that they are easily exchanged by other ions and/or by the solvent molecules. In contrast, the stronger binding of the pillaring cations to the oxide layer makes the 1050°C material intact against such an attack.

Cathode performances of layered MnO_2.—Table II summarizes the chemical composition and theoretical capacity of two materials. The theoretical capacities that were calculated by assuming a one-electron charge/discharge reaction are higher than that of spinel $Li_xMn_2O_4$ (148 mAh g^{-1}). The lower values in both the Mn valence and theoretical capacity in the 1050°C material come from the fact that manganese oxides favor oxygen-deficient phases at higher temperatures.[30] Also note the difference in the interlayer water content between two samples.

Figure 8 shows the cycling behavior of two cathodes that was obtained in the cathode-limited Li/PC + DME-$LiClO_4$/MnO_2 cells. The initial discharge capacity is higher with the 800°C material as expected from its theoretical value. For the cathode cyclability, however, the 1050°C material outperforms the 800°C one. Figure 9 shows the galvanostatic charge/discharge potential profiles recorded with the two cathodes, where the curves of the 1st and 41st cycle are represented. In each trace, the top one corresponds to the charging curve and the bottom one to the discharging curve. The two cathodes show a similar potential profile at the 1st cycle but far different ones at the 41st cycle. In particular, the charge and discharge near 4.0 V are apparent in the 800°C cathode at the 41st cycle. A comparison of the charge/discharge profiles of the two cathodes also reveals that the potential difference between the charging and discharging curves is larger in the 1050°C cathode, suggesting that cell polarization is more serious in this electrode. This feature is discussed later after providing their cyclic voltammograms.

In Fig. 10, the XRD patterns are displayed that were obtained after the 20th charging. It is seen that the cell cycling leads to a substantial change in the XRD patterns in the 800°C material. The diffraction peaks belonging to the initial layered lattice disappear, but several unknown peaks develop with the highest peak at 18°. A similar XRD result has been reported in the literature, where the broad and strong 18° peak is attributed to the (111) diffraction of spinel phases that are generated from the layered Na_xMnO_2 after repeated

Downloaded 17 Jul 2009 to 147.46.182.184. Redistribution subject to ECS license or copyright; see http://www.ecsdl.org/terms_use.jsp

S0013-4651(99)06-148-0 CCC: $7.00 © The Electrochemical Society, Inc.

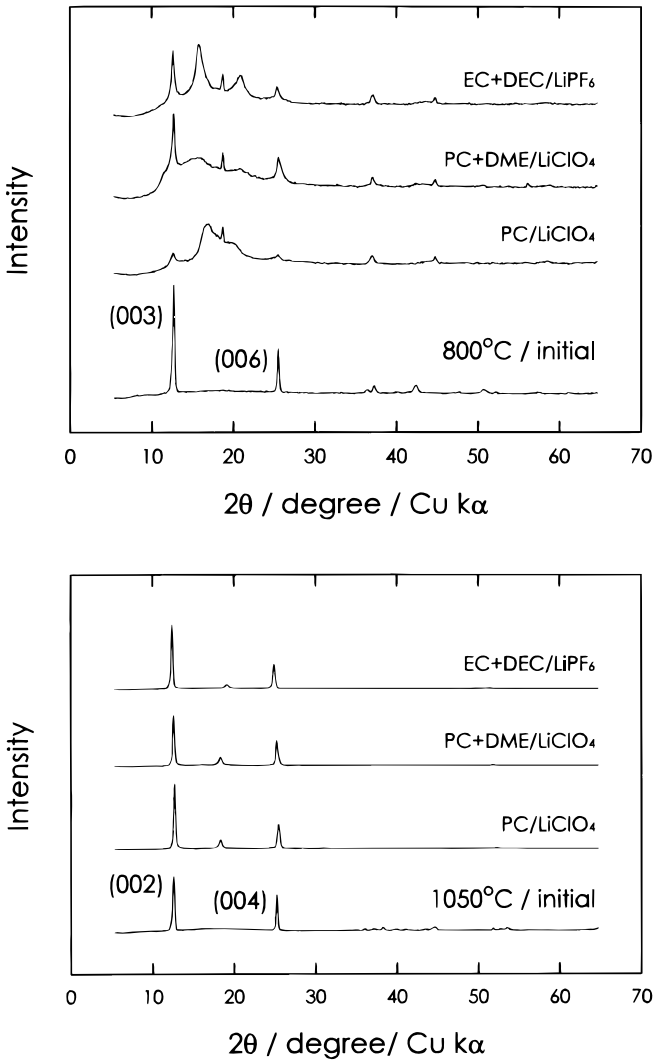

Figure 7. XRD patterns of the MnO_2 materials recorded after soaking in various electrolytes. Note that there appear new diffraction lines after soaking in the case of the 800°C material but a negligible change in the 1050°C material.

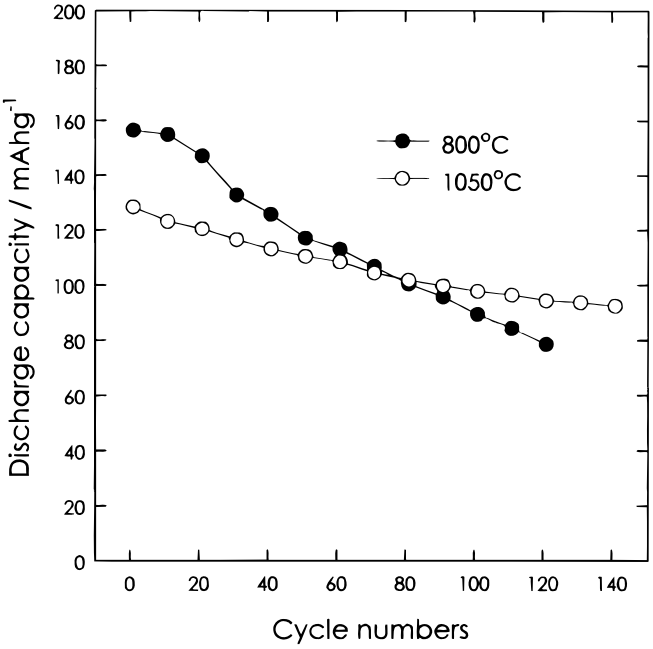

Figure 8. Discharge capacity of Li/PC + DME-$LiClO_4$/MnO_2 cells according to cycle numbers. Cycling was carried out galvanostatically at 1 mA cm^{-2} (0.4 C) at 2.0 to 4.3 V (*vs.* Li/Li^+). The cathodes were composed of MnO_2 powder, Ketjen Black, and PTFE binder (15:2:1 wt ratio).

cell cycling.[14] This observation is contrasted by the 1050°C material that maintains its structural integrity for long cycles. As seen in Fig. 10, the (00*l*) diffraction lines are still observed even if they become slightly broader than the initial ones.

Figure 11 shows the cyclic voltammograms recorded with the two cathodes, where the upper trace in each curve corresponds to the charging reaction and the bottom one to the discharging reaction. In the case of the 800°C-prepared MnO_2, only one redox pair is observed at 2.7 to 3.5 V in the 1st cycle. Upon cell cycling, however, additional redox pairs develop at around 4.0 V, of which the location and shape are very close to those of spinel $Li_xMn_2O_4$ electrodes.[31] From this and another observation whereby the cycled 800°C cathode gives the highest diffraction line at 18° (Fig. 10) like the spinel phases, it is very likely that this material transforms to spinel phases with cell cycling. In the meantime, as the spinel manganese oxide cathode also charges and discharges in the 3 V region; the redox pair located at 2.7 and 3.2 V may be assigned to that coming from the spinel phases. But as the initial layered MnO_2 cathode also charges and discharges in this potential region, this assignment is not very convincing.

The 1050°C cathode similarly gives rise to a redox pair at 3.7 to 4.0 V, but it differs from those observed with spinel-related phases in several features. First, the discharging peak is so broad and weak that it cannot be recognized. Second, the charging peak steadily moves to the positive direction in the range of 3.7 to 4.0 V with cell cycling. Third, it is not resolved into two peaks. One possible explanation on the nature of this redox pair has been provided in the literature, where this is attributed to the oxidation peak of interlayer water molecules.[32] Two observations made in this study, however, do not support this possibility. First, this peak is absent in the 800°C cathode even if this material also contains the interlayer water. Second, if this is the case, a decrease in the peak intensity is expected with cell cycling as the water is depleted with repeated oxidation. Contrary to this expectation, the results in Fig. 11 show a steady growth of this peak at 3.7 to 4.0 V with cell cycling. It is, therefore, more likely that this higher potential peak is relevant to the redox reactions involved in the MnO_2 itself.

Table II. Chemical composition and theoretical capacity of two layered MnO_2 materials.

Initial molar ratio *vs.* MnO(100)		Preparation temperature (°C)	Formula	Mn^{4+} (%)	Avg. Mn oxidation state	Theoretical capacity[a] ($mAh\ g^{-1}$)
KNO_3	LiOH					
50	10	800	$Li_{0.13}K_{0.34}MnO_{2.19}\cdot 0.27H_2O$	87.41	3.87	215
50	10	1050	$Li_{0.12}K_{0.35}MnO_{2.14}\cdot 0.45H_2O$	75.02	3.75	180

[a] Theoretical capacity based on a one-electron discharge/charge reaction.

Downloaded 17 Jul 2009 to 147.46.182.184. Redistribution subject to ECS license or copyright; see http://www.ecsdl.org/terms_use.jsp

S0013-4651(99)06-148-0 CCC: $7.00 © The Electrochemical Society, Inc.

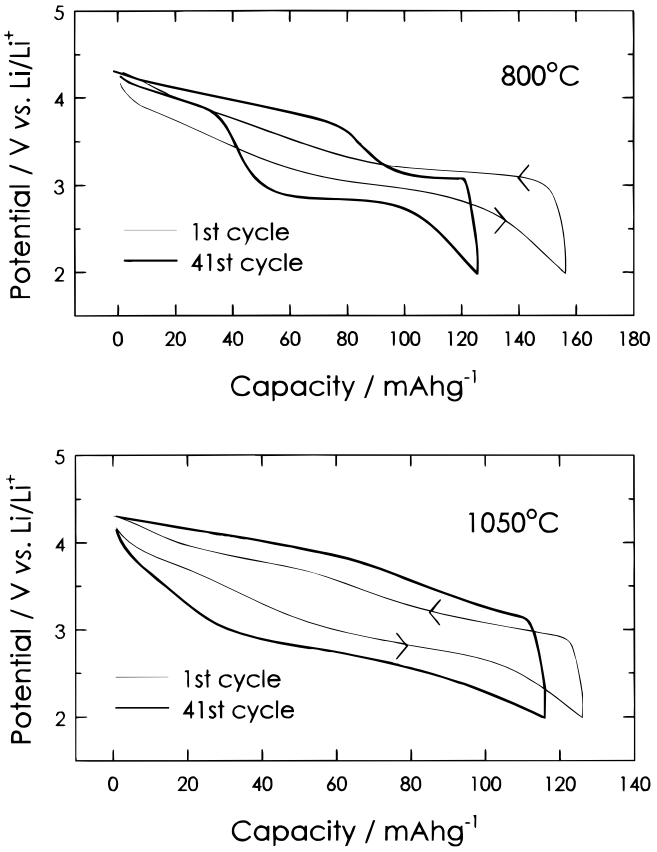

Figure 9. Galvanostatic charge/discharge potential profiles of the two MnO_2 cathodes. The cathode composition and cycling conditions were the same as for Fig. 8.

The results in Fig. 11 also show that the potential difference between the oxidation and reduction peaks, more prominently, between the redox pair located in the lower potential region, is larger in the case of the 1050°C cathode. The larger cell polarization, which is also evident in the galvanostatic charge/discharge profiles (Fig. 9), is seemingly caused by a sluggish Li^+ intercalation in this material. The narrower gallery space and higher population of pillaring species may retard Li^+ intercalation in the 1050°C material.

The transformation from the 800°C-prepared MnO_2 to spinel phases can be explained as follows. In transition metal oxide cathodes, the Li^+ intercalation and deintercalation process is often accompanied by a lattice volume change and reordering of metal ions within the lattice.[33] In the case of manganese oxides, the reordering/mixing between the Li and Mn ions can easily occur because of the similarity in their size.[15,16,21] In particular, as the layered MnO_2 prepared at 800°C in this work has the same oxide packing pattern as the spinel phases, the transition can readily occur without any rearrangement in the oxide framework. By contrast, the structural transition between those having different oxide-packing patterns, for example, the P2-O3 (from the 1050°C-prepared MnO_2 to spinels) and O2-O3 transition, is not likely because a high energy is required for the breakdown of metal-oxide bonds and lattice rearrangement.[34,35] For example, the P2-type layered $Na_{0.70}MnO_{2+y}$ and Na_xCoO_2 are reported to be inert to the spinel transition.[35]

Figure 12 shows the chemical compositions of two cathode materials that were analyzed after cell cycling. As seen, the 800°C material rapidly loses K^+ ions from the gallery space but the K^+ loss is less significant from the 1050°C material. In the meantime, some Mn loss from both cathodes is noted, suggesting that some portion of capacity loss comes from the material loss due to the dissolution.[5-7] However, as the Mn loss from both cathodes is largely the same, the difference of cathode cyclability can be ascribed to the difference in the degree of K^+ leaching and the concomitant structural breakdown.

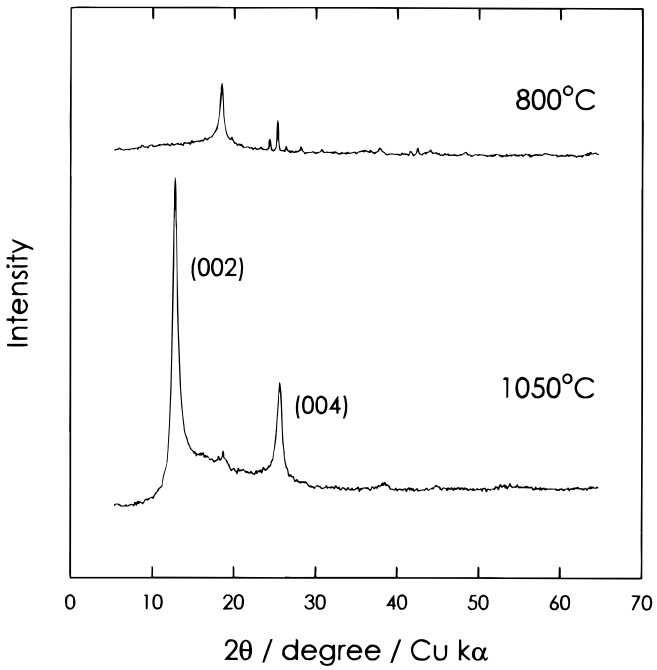

Figure 10. XRD patterns of the composite cathodes recorded after 20 cycles. Note that the diffraction lines that are present in the fresh state (see Fig. 2) largely disappear but a new diffraction line develops at 18° in the 800°C cathode.

Conclusions

In this study, two layered MnO_2 materials having different crystal structure were prepared, and their cathode performance in 3 V Li/PC + DME-$LiClO_4$/MnO_2 secondary cells was investigated. Of particular interest was the identification of the factors controlling the structural stability and spinel transition tendency in the layered MnO_2 materials.

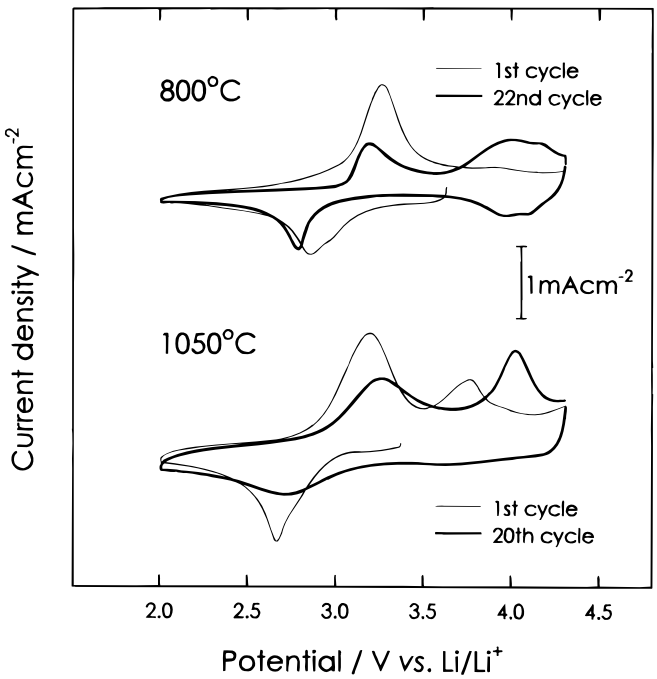

Figure 11. Cyclic voltammograms traced with two cathodes. Scan rate = 0.1 mV s^{-1}. Note two redox pairs appearing at 4.0 V (*vs.* Li/Li^+) in the 800°C cathode. The cathode composition and cycling conditions were the same as for Fig. 8.

Downloaded 17 Jul 2009 to 147.46.182.184. Redistribution subject to ECS license or copyright; see http://www.ecsdl.org/terms_use.jsp

S0013-4651(99)06-148-0 CCC: $7.00 © The Electrochemical Society, Inc.

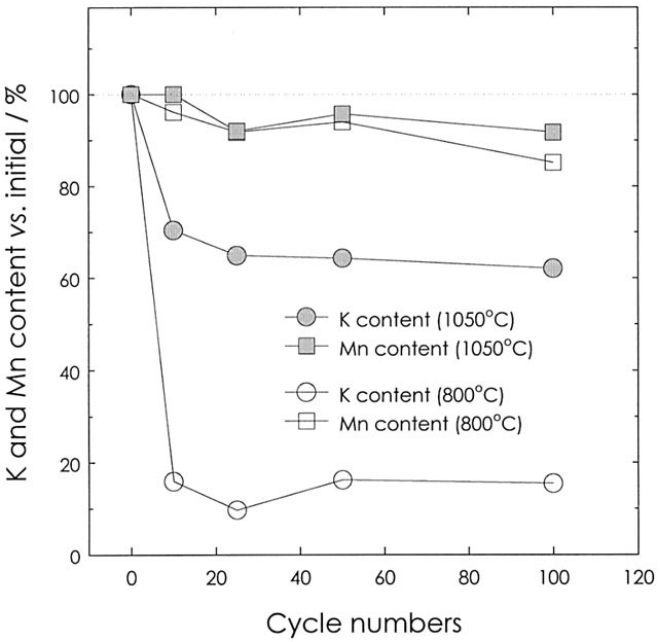

Figure 12. Variation of K and Mn contents in the cathode materials with cell cycling. The cathode composition and cycling conditions were the same as for Fig. 8. The chemical compositions were normalized against those observed in the fresh state.

The layered MnO_2 prepared at 800°C has a trigonal $R\bar{3}m$ symmetry with O3-type oxide-packing pattern. Due to the wider gallery space, the pillaring K^+ ions are liable to be easily leached out. As a result of structural instability, the layered framework is largely destroyed with cell cycling, leading to severe capacity loss. Also, due to the similarity of oxide-packing pattern to the spinel phase, it readily transforms to the spinel phases.

In contrast, the 1050°C material has an orthorhombic *Cmcm* symmetry with P2-type oxide packing, which is far different from that of the spinel. As the gallery space is narrower, the pillaring K^+ ions are relatively immobile. This stronger pillaring effect imparts a structural stability to this material. The layered lattice persists even after prolonged cell cycling. The spinel transformation is absent as its oxide-packing pattern is different to that of the spinel phase.

Finally, the mobility of pillaring cations and the type of oxide-packing patterns turn out to be the most important factors controlling the stability of the layered MnO_2 structure and the tendency for spinel transition.

Acknowledgment

This study was supported by Korean Ministry of Education through Research Fund.

References

1. J. Desilvestro and O. Haas, *J. Electrochem. Soc.*, **137**, 5C (1990).
2. T. Ohzuku and A. Ueda, *Solid State Ionics*, **69**, 201 (1994).
3. T. Ohzuku, in *Lithium Batteries, New Materials, Developments and Perspectives*, G. Pistoia, Editor, Chap. 6, Elsevier, New York (1994).
4. R. Koksbang, J. Barker, H. Shi, and M. Y. Saidi, *Solid State Ionics*, **84**, 1 (1996).
5. D. H. Jang, Y. J. Shin, and S. M. Oh, *J. Electrochem. Soc.*, **143**, 2204 (1996).
6. D. H. Jang and S. M. Oh, *J. Electrochem. Soc.*, **144**, 3342 (1997).
7. D. H. Jang and S. M. Oh, *Electrochim. Acta*, **43**, 1023 (1998).
8. G. Pistoia, *J. Electrochem. Soc.*, **129**, 1861 (1982).
9. S. H. Kim and S. M. Oh, in *Proceedings of the 1st Korea-Japan Joint Seminar on Advanced Batteries*, p. 127, Seoul, Korea (1996).
10. S. H. Kim and S. M. Oh, *J. Power Sources*, **72**, 150 (1998).
11. S. H. Kim, S. J. Kim, and S. M. Oh, *Chem. Mater.*, **11**, 557 (1999).
12. S. H. Kim and S. M. Oh, in *Proceedings of the 9th International Meeting on Lithium Batteries*, Edinburgh, U.K. (1998).
13. G. Vitins and K. West, *J. Electrochem. Soc.*, **144**, 2587 (1997).
14. F. Le Cras, S. Rohs, M. Anne, and P. Strobel, *J. Power Sources*, **54**, 319 (1995).
15. R. Chen and M. S. Whittingham, *J. Electrochem. Soc.*, **144**, L64 (1997).
16. C. Delmas, in *Lithium Batteries, New Materials, Developments and Perspectives*, G. Pistoia, Editor, Chap. 12, Elsevier, New York (1994).
17. A. Sakthivel and R. A. Young, *User's Guide to Programs DBWS-9006 and DBWS-9006PC*, Georgia Institute of Technology, Atlanta, GA (1990).
18. G. H. Jeffery, J. Bassett, J. Mendham, and R. C. Denney, *Vogel's Textbook of Quantitative Chemical Analysis*, 5th ed., p. 584, Longman, Harlow, U.K. (1989).
19. J. E. Post and D. R. Veblen, *Am. Mineral.*, **75**, 477 (1990).
20. S. Bach, J.-P. Pereira-Ramos, C. Cachet, M. Bode, and L. T. Yu, *Electrochim. Acta*, **38**, 1695 (1993).
21. R. Chen, P. Zavalij, and M. S. Whittingham, *Chem. Mater.*, **8**, 1275 (1996).
22. M. H. Rossouw, D. C. Liles, and M. M. Thackeray, *J. Solid State Chem.*, **104**, 464 (1993).
23. P. Le Goff, N. Baffier, S. Bach, J.-P. Pereira-Ramos, and R. Messina, *J. Mater. Chem.*, **4**, 133 (1994).
24. P. Le Goff, N. Baffier, S. Bach, J.-P. Pereira-Ramos, and R. Messina, *J. Mater. Chem.*, **4**, 875 (1994).
25. A. R. Armstrong and P. G. Bruce, *Nature*, **381**, 499 (1996).
26. F. Capitaine, P. Gravereau, and C. Delmas, *Solid State Ionics*, **89**, 197 (1996).
27. J.-P. Parant, R. Olazcuaga, M. Devalette, C. Fouassier, and P. Hagenmuller, *J. Solid State Chem.*, **3**, 1 (1971).
28. R. E. Marsh and F. H. Herbstein, *Acta Crystallogr., Sect. B*, **39**, 280 (1983).
29. P. Strobel, J. Durr, M. H. Tuiler, and J. C. Charenton, *J. Mater. Chem.*, **3**, 453 (1993).
30. T. E. Moore, M. Ellis, and P. W. Selwood, *J. Am. Chem. Soc.*, **72**, 856 (1950).
31. T. Ohzuku, M. Kitagawa, and T. Hirai, *J. Electrochem. Soc.*, **137**, 769 (1990).
32. F. Leroux, D. Guyomard, and Y. Piffard, *Solid State Ionics*, **80**, 307 (1995).
33. M. M. Thackeray, *J. Electrochem. Soc.*, **142**, 2558 (1995).
34. A. Mendiboure, C. Delmas, and P. Hagenmuller, *Mater. Res. Bull.*, **19**, 1383 (1984).
35. A. Mendiboure, C. Delmas, and P. Hagenmuller, *J. Solid State Chem.*, **57**, 323 (1985).

Downloaded 17 Jul 2009 to 147.46.182.184. Redistribution subject to ECS license or copyright; see http://www.ecsdl.org/terms_use.jsp